



Selective dealkylation of alkyl polycyclic aromatic hydrocarbons towards innovative upgrading process of practical heavy oil

Journal:	<i>Catalysis Science & Technology</i>
Manuscript ID	CY-ART-08-2020-001590.R1
Article Type:	Paper
Date Submitted by the Author:	17-Oct-2020
Complete List of Authors:	Nakano, Fumiya; Tottori University, Center for Research on Green Sustainable Chemistry Goma, Tomohide; Tottori University, Center for Research on Green Sustainable Chemistry Suganuma, Satoshi; Tottori University, Center for Research on Green Sustainable Chemistry Tsuji, Etsushi; Tottori University, Center for Research on Green Sustainable Chemistry Katada, Naonobu; Tottori University, Center for Research on Green Sustainable Chemistry

Selective dealkylation of alkyl polycyclic aromatic hydrocarbons towards innovative upgrading process of practical heavy oil

Fumiya Nakano, Tomohide Goma, Satoshi Suganuma,* Etsushi Tsuji, Naonobu Katada

Center for Research on Green Sustainable Chemistry, Tottori University, 4-101 Koyama-cho Minami, Tottori

680-8552, Japan

Phone: +81-857-31-5256; Fax: +81-857-31-5684; E-mail: suganuma@tottori-u.ac.jp

Keywords

Alkyl polycyclic aromatic hydrocarbon; dealkylation; silica monolayer solid acid catalyst; heavy oil

Abstract

Dealkylation of alkyl polycyclic aromatic hydrocarbons (APAHs) in vacuum gas oil (VGO) was studied as a novel upgrading process alternative to conventional processes. A silica-monolayer loaded on alumina (SMA) with weak Brønsted acid sites and large pore size exhibited higher activity than amorphous silica-alumina and zeolites (USY and ZSM-5). SMA almost completely converted the APAHs into aromatics and alkanes, but a small amount of APAHs with methyl and ethyl groups (short-chain) were unreacted. Larger pore size of SMA was proposed to be enough for bulky APAHs to diffuse. The dealkylation by SMA formed large amounts of long-chain alkanes, which can be utilized as light oil and kerosene for fuel, lubricating oil, etc. The cracking of long-chain alkanes did not proceed, and thus scarcely formed lighter alkanes. SMA in the reaction adsorbed alkanes but did not form coking, and therefore exhibited continuous dealkylation activity. Additionally, it was revealed that the pore size of SMA slightly affected the composition of the formed alkanes.

1. Introduction

Petroleum refining is generally developed for the production of transportation fuels, but perform minor but essential production of building blocks for petrochemicals, such as light alkenes (ethylene and propylene) and BTEX (benzene, toluene, ethylbenzene, and xylenes) ¹⁻⁴. The transportation fuels are produced by atmospheric distillation, while the atmospheric residue oil is processed by vacuum distillation. The vacuum gas oil (VGO) is converted into gasoline, light oil, and kerosene by fluid catalytic cracking (FCC), hydrocracking, or thermal cracking. However, the growing rate of demand in transportation fuel is declining due to improvement of fuel consumption of vehicles and control of carbon dioxide emission ⁵. Yield of the petrochemicals is limited based on the operation conditions, which are designed to fit the demands of transportation fuel. Recently, an FCC process has been developed for increasing production of light alkenes, but yield of benzene derivatives cannot be increased by further reorganization of the process. On the other hand, the hydrocracking process consumes a large amount of hydrogen for hydrogenation of polycyclic aromatic hydrocarbons, which leads to a decrease of benzene derivative yields due to the severe hydrogenation condition. Benzene derivatives are applied as the chemicals and their intermediates of synthetic fibers, resins, detergents, and various organic ingredients. Among the benzene derivatives, the manufacture volumes of benzene and paraxylene are notably increasing. However, production of benzene derivatives is complicated for FCC and hydrocracking. Therefore, innovation of petroleum refining for increasing flexibility in the production is strongly required, in order to cope with the change of situation.

We have studied an alternative process to FCC and hydrocracking ⁶⁻⁹, and an outline was given in a review ¹⁰. The components in VGO are categorized into 3 main types: aliphatics (alkanes as main components), aromatics, and alkylaromatics. If the alkyl polycyclic aromatic hydrocarbons (APAHs) are completely dealkylated to alkanes and PAHs with no alkyl groups, the components can be facily separated into 2 types by such methods as solvent extraction ¹¹⁻¹³. The dealkylation of an APAH via β -scission of a carbenium ion is catalyzed by Brønsted acid sites, like cracking of cumene (2-phenylpropane) ^{14,15}, forming an aromatic hydrocarbon and a carbenium ion. Then, alkanes are formed from the carbenium ions through the presumed reaction pathways as follows: hydrogenation of generated alkene from the carbenium ion or hydride transfer from the other alkane to the

carbenium ion. If the alkane produced from APAHs is not cracked but keeps the long chain length, the yield of middle distillates such as light oil, kerosene, and >C₂₀ alkanes for lubricating oil can be maximized. On the other hand, the produced polycyclic aromatic hydrocarbons such as naphthalene, anthracene, phenanthrene, pyrene, etc. can be converted by partial hydrogenation of the aromatic rings into tetralin derivatives, e.g., naphthalene into tetralin¹⁶⁻¹⁸. Then, tetralin derivatives are converted into benzene derivatives through ring-opening^{19,20}. In fact, BTX production from PAHs has been recently reported²¹⁻²³. Thus, this alternative process to the conventional processes can maximize the amounts of long-chain alkanes and benzene derivatives with the minimum consumption of hydrogen, compared to the hydrocracking process. We have previously reported the dealkylation as a model reaction, in which only the C₁₆ and 18 alkylnaphthalenes were fed as the reactant⁶. The next report revealed the influence of coexisting substances in VGO as real heavy oil on the conversion of C₁₆ alkylnaphthalene added as an index reactant⁷. However, the reactivity of original hydrocarbons in VGO has not been apparent. It is essential for a commercialized process to comprehend the change of carbon balance in the reaction.

In this study, dealkylation of APAHs in practical VGO is made solely to proceed over various solid acids under hydrogen atmosphere. However, the solid acids are poisoned by basic nitrogen-containing compounds in the original VGO. Before the dealkylation, the basic nitrogen-containing aromatic hydrocarbons were removed by acidic ion-exchanged resins (containing a SO₃H group)⁷. The industrial utilization of this resin may be difficult due to the expensiveness and the laborious regeneration, but we have recently found that the alternative to the resin was inexpensive amorphous silica-alumina, which could be simply regenerated by heating⁸. Benzene was added for increasing the fluidity. However, actual processes were operated in a flow of high-viscosity crude oil, and our dealkylation process should be also applied at large scales without addition of benzene. The dealkylation activity was compared among aluminosilicates: such as amorphous silica-alumina, zeolites, and a silica monolayer loaded on alumina (SMA) as a candidate of catalyst. SMA can be synthesized by chemical vapor deposition (CVD) of Si precursor on the surfaces of alumina and has been found to have catalytic activity for Brønsted acid-catalyzed reactions^{24,25}. SMA with 8–12 nm⁻² of the Si concentration showed high activity and selectivity for dealkylation of C₁₆, 18 alkylnaphthalene into naphthalene and C₁₆, 18 alkanes⁶. Therefore, SMA with 8 nm⁻² of the Si

concentration were prepared for the dealkylation of APAHs in the practical VGO. Additionally, it was presumed that the textural properties of SMA affected the dealkylation activity in the practical VGO, which contained bulky hydrocarbons to prevent the diffusion of the reactants. In order to investigate the influence of pore size on dealkylation activity, SMA with different pore sizes from 6.2 to 33 nm were synthesized. In the reaction, a small amount of hydrogen is fed for hydrogenation of the alkenes, which are produced by the dealkylation and contained in the practical oil, because formation of coke from the alkenes deactivates the solid acid. The previous study mainly reported the reactivity of C16, 18 alkylnaphthalene, as a model reactant for indexing the dealkylation rate, in the coexistence of VGO components to quantitatively show the activity of SMA catalyst ⁷, and here the reactivity and selectivity of dealkylation of practical VGO components are evaluated with the aid of the two-dimensional GC (2D-GC) technique, in order to clarify changes in compositions of existing hydrocarbons in VGO. The high dealkylation activity and selectivity of long-chain alkanes of SMA, due to weak Brønsted acidity and large pore size, will be focused on.

2. Experimental

2.1. Catalyst preparation

Thin silica layers were prepared by means of a CVD (chemical vapor deposition) method ²⁵ on the alumina materials JRC-ALO-6, -7, and -9, which had been supplied by Catalysis Society of Japan as reference catalysts, and a purchased sample from FUJIFILM Wako Pure Chemical Corp. The deposition was performed in a vacuum system using Si(OCH₃)₄ (tetramethoxysilane) as the precursor of silica. After evacuation of the support alumina at 673 K for 2 h, vapor of tetramethoxysilane was admitted contacting with alumina at 593 K, and the resultant increase of weight was monitored using a quartz spring balance. The supply of tetramethoxysilane vapor and evacuation were repeated to feed the precursor vapor and to remove the gaseous products continuously. The degree of vacuum was ca. 10⁻³ Torr (1 Torr = 133.3 Pa), and the vapor pressure of alkoxide was kept at ca. 2.5 Torr by chilling the reservoir with an ice bath. After a weight increase corresponding to SiO₂ with ca. 8 nm⁻² of the Si concentration was observed, the sample was calcined in oxygen (200 Torr) at 673 K for 12 h. The amount of deposited Si was calculated from the weight increase while assuming that the formed material was SiO₂, and the

samples with ca. 8-9 Si atoms nm⁻² were employed in the present study; hereafter, they are called SMA (silica monolayer loaded on alumina). As a comparison, an amorphous silica-alumina catalyst industrially available, N631-L (JGC Catalysts and Chemicals Ltd.), was tested for catalytic and analytical experiments, as well as the following zeolites. An H-USY zeolite CBV720 with FAU structure (Si/Al₂= 29) was supplied by Zeolyst. In addition, an NH₄-ZSM-5 zeolite HSZ820NAA with MFI structure (Si/Al₂= 22) was supplied by Tosoh Corp; it was converted into H-ZSM-5 in the pretreatments for analytical and catalytic experiments.

2.2. Structural analysis

The nitrogen adsorption isotherm was measured at 77 K using BELSorp-max equipment (Microtrac-BEL) after pretreatment at 573 K for 1 h. The surface area was calculated by the BET (Brunauer-Emmett-Teller) equation²⁶, and the pore diameter distribution was analyzed from the desorption branch using a BJH (Barrett-Joyner-Halenda) method²⁷.

The amount of chemisorbed benzoate anion was measured by a BAT (benzaldehyde-ammonia titration) method²⁸. About 40 mg of the sample was packed in a Pyrex tube (4 mm i.d.) and pretreated in an oxygen flow (27 μmol s⁻¹, atmospheric pressure) at 673 K for 1 h. Benzaldehyde (9.8 μmol) was injected into the sample bed at 573 K in a helium flow (27 μmol s⁻¹, atmospheric pressure), and the eluted aldehyde was monitored by a GC (GC-8A, Shimadzu) with a silicone SE-30 packed column and an FID (flame ionization detector). The injection of the aldehyde was repeated several times until the saturation of adsorption was observed, and then ammonia (0.41 mmol) was repeatedly supplied at 673 K. The formed benzonitrile was quantified by the GC, and the coverage was calculated on the assumption that the benzoate anion was adsorbed only on the exposed alumina surface, not on the silica-covered surface²⁵.

The ammonia IRMS (infrared / mass spectroscopy) -TPD (temperature-programmed desorption) method was applied to measure the number and strength distribution of each of the Brønsted and Lewis acid sites²⁹. A self-supporting disc (1 cm diameter), molded from the sample by compression, was held by a set of metal rings to fix in a cell of Microtrac-BEL IRMS-TPD analyzer and pretreated at 823 K in oxygen. The IR (infrared) spectra were collected by an IR spectrometer (JASCO, FT/IR-4200) equipped with an MCT (mercury cadmium telluride

detector) while heating the sample in a helium flow ($68 \mu\text{mol s}^{-1}$, 6 kPa) at 2 K min^{-1} . Then ammonia was adsorbed at 343 K, and the sample was again heated under the same conditions. The IR spectra and MS response (measured by Pfeiffer Vacuum QMG220) were recorded. The ammonia TPD profile of each of the Brønsted and Lewis acid sites was analyzed according to our previous study³⁰. The number of acid sites was calculated from the peak intensity of the TPD, and the distribution of enthalpy of ammonia desorption (so-called adsorption heat) was analyzed by the curve fitting method³¹.

2.3. Dealkylation of APAHs

The reactant for dealkylation of APAHs was prepared as follows. An isomer mixture of hexadecyl-naphthalene (HDN) with one alkyl branch, whose carbon number was 16, was purchased from Exxon Mobil Corp. as a commercial sample Synesstic 5. VGO, yielded by vacuum distillation of a Middle East origin crude oil (final boiling point at 1008 K, specific gravity 0.915 g cm^{-3} , C: 85.11 wt%, H: 12.35 wt%, S: 2.35 wt%, N: 0.06 wt%), was mixed with benzene and the above HDN. The composition of VGO:benzene:HDN was 1:1:0.11 in weight ratio. Here benzene was added for increasing the fluidity, in order to mix the resulting VGO with adsorbent for the removal of basic compounds and to feed it with a pump for the reaction tests. HDN was added as an index reactant for quantitative evaluation of catalytic activity for the dealkylation of APAHs. Then, for the removal of basic compounds, a cation exchange resin (Amberlyst-15DRY, purchased from Organo) after pretreatment at 353 K overnight was added into the VGO; 10 wt% of Amberlyst-15DRY based on the VGO was used. The resulting mixture was stirred at room temperature for 1 h, and then the Amberlyst-15DRY was removed by filtration. The above cation exchange resin treatment was repeatedly carried out (usually 2-3 times) until the pH trend indicated the neutralization point as observed using an automatic neutralization titrator (916Ti-Touch, Metrohm AG)^{7,8}.

The reaction was carried out by a fixed-bed continuous-flow method. The catalyst was packed in a stainless steel tube (4 mm i.d.). The catalyst (210 mg) was pretreated in a flow of hydrogen (0.12 mol h^{-1}) under atmospheric pressure at 773 K for 1 h. Then, the reactant was fed at 1.2 g h^{-1} with a hydrogen flow (0.12 mol h^{-1}) through the catalyst bed at 723 K. The total pressure in the tube was kept at 1 MPa using a back pressure valve

connected to the outlet. The formed material was trapped in a glass tube chilled with an ice bath. The products were analyzed using a 2D-GC (Agilent 7890) with an FID and two capillary columns (0.25 μm thickness DB-5MS, length 30 m, i.d. 0.250 mm, and 0.15 μm thickness DB-17HT, length 5 m, i.d. 0.250 mm). An internal standard method was adopted with tetraethylene glycol dimethyl ether as the standard compound added after collecting the products. The composition of the components based on the number of carbon atoms was calculated from the relative intensities of GC peaks:

$$\text{composition} = \frac{\text{amount of carbon in each components in liquid (c - mol)}}{\text{amount of carbon in feedstock (c - mol)}} \times \text{fraction of recovered liquid}$$

HDN conversion was calculated as follows:

$$\text{conversion} = \frac{\text{amount of recovered HDN in liquid (c - mol)}}{\text{amount of feeded HDN (c - mol)}} \times \text{fraction of recovered liquid}$$

Light hydrocarbons were recovered by a gas pack and analyzed using GC equipment (GC-2014, Shimadzu) with an FID and a capillary column (InertCap1, 5.0 μm thickness, 30 m in length, and internal diameter of 0.53 mm). The composition averaged during 2-8 h of the time on stream was calculated:

$$\text{composition} = \frac{\text{amount of carbon in each components in gas (c - mol)}}{\text{amount of carbon in feedstock (c - mol)}} \times \text{fraction of recovered gas}$$

The structure and composition of residues adsorbed on the catalysts after the reaction were investigated with elemental analysis and infrared (IR) spectroscopy. The catalysts were recovered after the reaction and dried at room temperature under vacuum. An elemental analysis of the catalysts was carried out with a Vario EL cube (Elementar Analytical). In the IR measurement, a self-supporting disc (1 cm diameter) was molded from a ground mixture of the catalyst and potassium bromide (1:10 in weight ratio). It was set in a Microtrac BEL, IRMS-TPD analyzer. After removal of water adsorbed on the catalyst under vacuum at 473 K for 0.5 h, the IR spectrum was recorded under vacuum at 293 K.

3. Results

3.1. Physical properties and acidity profiles

Table 1 shows physical properties of the silica monolayer deposited on alumina (SMA). The amount of deposited material is here indicated by the surface concentration (Si atoms nm^{-2}). The coverage of surface by silica

was calculated by the BAT method. At $8.3 \pm 0.4 \text{ nm}^{-2}$, the coverage of all the SMA samples exceeded 85%. It tells us that a monolayer of silica with 1:1 Al-O-Si bonding was formed to cover almost completely the Al_2O_3 surface^{25,32}. BET surface areas of SMA before and after silica deposition are indicated in **Table S1** and **Table 1**, respectively. The BET surface area of SMA (after the CVD) divided by the weight of alumina was not largely different from the value before silica deposition, in all the cases, indicating that the surface area was unchanged by the CVD. The mean pore diameter and mesopore volume of SMA before and after silica deposition are also shown in **Table S1** and **Table 1**, respectively, and the pore size distribution in the mesopore region is shown in **Figure S1**. The pore size and its distribution of SMA were generally close to those of the original Al_2O_3 . The order in mode value of pore size was SMA-1 (6.2 nm) < SMA-2 (9.2 nm) < SMA-3 (24 nm) < SMA-4 (33 nm), according to the pore sizes of parent Al_2O_3 . The mesopore volume increased with increasing the pore size. These textural profiles indicate that the morphology of particles was retained, consistent with that a very thin layer of silica was formed on alumina. The physical properties of amorphous silica-alumina (N631-L) and the zeolites (USY and ZSM-5) are indicated in **Table 2**. The BET surfaces of amorphous silica-alumina and zeolites were higher than those of SMAs. The mesopore size of N631-L was smaller than those of SMAs. On the other hand, most of the active sites on the zeolites are estimated to exist in the micropores, and the sizes of micropore channels in USY and ZSM-5 were ca. 0.7 nm and 0.6 nm, respectively, far smaller than the pores of SMAs and N631-L. The mesopore volume of N631-L was similar to SMA-1, while the zeolites possessed small volumes of mesopores, mainly located between the crystal grains.

The ammonia IRMS-TPD determined the acidic properties³⁰. **Figures S2** and **S3** show the IR spectra obtained on the catalysts during the TPD experiments. A sharp band at ca. 1450 cm^{-1} was assigned to bending (ν_4) vibration of NH_4^+ adsorbed on Brønsted acid sites (NH_4^+ (BAS)). A small peak at $1250\text{-}1330 \text{ cm}^{-1}$ was assigned to bending (δ_s) vibration of ammonia adsorbed on Lewis acid sites (ammonia (LAS)). **Figure S4** shows TPD profiles of ammonia desorbed from the acid sites. MS-TPD indicates the profile of ammonia desorption evaluated with mass spectroscopy. The TPD profiles were calculated from the IR-TPD of ca. 1450 cm^{-1} -band (ν_4 , NH_4^+ (BAS)) and $1250\text{-}1330 \text{ cm}^{-1}$ -band (δ_s , ammonia (LAS)), respectively³⁰. **Table 3** shows the amount and strength of BAS. Mode value in enthalpy (ΔH) of ammonia desorption from the BAS on catalysts is indicated as an index of

Brønsted acid strength (distribution of ΔH is shown in **Figure S5**)³³. No difference was found in the strength of BAS on the SMAs as shown by ΔH . The amount of BAS on SMA distributed in 0.06-0.11 mol kg⁻¹ (0.25-0.36 nm⁻² on the surface area basis). The amorphous silica-alumina (N631-L) had more than 1.5 times the BAS of SMAs, and the acid strength on N631-L was higher than those on SMAs. The amount of BAS on the zeolites (USY and ZSM-5) was more than SMAs and N631-L, and BAS on the zeolites was much stronger as estimated from ΔH . Especially, ZSM-5 possessed stronger BAS in a high density.

3.2. Dealkylation of alkyl aromatic hydrocarbons

SMA-3 exhibited high activity and selectivity in the model reaction of HDN as previously reported⁶, and was thus compared with various aluminosilicates as solid acids in this section. Hexadecylnaphthalene (HDN) was added to VGO as an index reactant, and the reactivity was assessed by the conversion of this compound. **Figure 1** shows the time courses of HDN conversion on various solid acids. At 2 h of the time on stream, all the catalysts showed almost equivalent conversion values. Decline in the reaction rate was in the order of N631-L < SMA-3 < USY << ZSM-5. Here it is noted that the previous studies have revealed the highest activity of SMA for the conversion of HDN at 673 K among the solid acids which were tested also in the present study^{6,7}. The present experiments were performed at 723 K for evaluation of the catalytic performances under practical conditions, and therefore the apparent order of conversion was somewhat different.

This study quantified not only the HDN conversion but also changes in the hydrocarbon compositions by the reaction over aromatics and aliphatics. The compositions of the products in the reactions on the catalysts are shown in **Tables S2-S5**. The time courses of composition of APAHs in outlet products are shown in **Figure 2**. The original (fed) VGO contained 32 c-mol% of APAHs including HDN. SMA-3 reduced the APAHs content down to 8 c-mol% constantly at 2-8 h of the time on stream, indicating that dealkylation of APAHs proceeded, and the catalytic activity was stably maintained. On N631-L and USY, the recovery of APAHs was high at the initial stage of the flow reaction, indicating the low activity, and the recovery decreased with the time on stream. On ZSM-5, more than half of the APAHs was eluted at the initial stage (2-4 h of the time on stream), showing the low activity, and the recovery gradually increased with the time on stream, indicating quick deactivation of the catalyst. These

results indicate that the dealkylation activity of SMA-3 was higher than those of the amorphous silica-alumina and zeolites. However, 8 c-mol% of the APAHs was unreacted even on SMA-3. **Figure S6** shows composition of alkyl groups in alkyl bicyclic and tricyclic aromatics in the products over SMA-3 during 2-8 h of the time on stream. Most of the side chains before the reactions possessed >5 carbon atoms in an alkyl group. The dealkylation on SMA-3 reduced the carbon number down to <5. It means that the APAHs with long-chain alkyl groups were mainly dealkylated, while the methyl and ethyl groups attached to the polyaromatic rings showed lower reactivity on SMA-3.

Figure 3 shows the time courses of composition of alkylbenzenes (alkyl monocyclic aromatics) in outlet products. The original VGO contained 9 c-mol% of alkylbenzenes. SMA-3 reduced alkylbenzenes in a small amount down to 7 c-mol%, while the amorphous silica-alumina and zeolites obviously increased the alkylbenzenes. More than half of outlet liquid and gas eluted in the reaction on ZSM-5 were alkylbenzenes in the initial period, but the yield decreased with the time on stream. Composition of the side chains in alkylbenzenes in the products on SMA-3 is displayed in **Figure S7**. Most of the alkylbenzenes in the products possessed long-chain alkyl groups, meaning that the alkyl monoaromatics were inactive regardless of the long chain length on SMA-3. It was in contrast to the observations in the case of APAHs as stated above; the chain length of the alkyl group affected the reactivity in the case of APAHs. It is concluded that SMA-3 was active for the dealkylation of APAHs with long-chain alkyl groups but inactive for the reactions of alkyl monoaromatics and APAHs with short-chain alkyl groups.

Figure 4 shows the time courses of composition of the alkanes in the products. The original VGO contained 56 c-mol% of long-chain aliphatics (>C₂₀); here it is noted that the original VGO contained alkanes and alkenes, whereas the outlet products contained mainly alkanes due to the reaction in pressurized hydrogen. ZSM-5 markedly decreased the >C₂₀ alkanes, suggesting the progress of cracking of alkane. USY and N631-L also showed decreases of >C₂₀ alkanes composition. SMA-3 also reduced the >C₂₀ alkanes, but the extent was less than the amorphous silica-alumina and zeolites to keep the composition at 44 c-mol% during 5-8 h (**Figure 4 (A)**). On the other hand, the original VGO contained only 4 c-mol% of C₁₀₋₂₀ alkanes and no <C₅ alkanes. Formation of <C₂₀ alkanes presumably due to the dealkylation of aromatics was observed as shown in **Figure 4 (B)** and **(C)**.

SMA-3 and N631-L produced more C10-20 alkanes than the zeolites, while C5-9 alkanes were produced in the following order: N631-L > USY \approx SMA-3 > ZSM-5. **Figure 5** shows the composition of light hydrocarbons during 2-8 h of the time on stream. The yield of light hydrocarbons was in the following order: SMA-3 < N631-L < USY < ZSM-5. The composition of C4-6 in the light hydrocarbons over SMA-3, N631-L, and USY was >60%, while ZSM-5 produced excessive amounts of C1-3 alkanes. Here it is emphasized that ZSM-5 did not produce C5-20 alkanes but C3-4 alkanes in large quantities.

A gradual decline in the dealkylation activity was observed as displayed in **Figures 1 and 2**. The substances adsorbed on the catalysts during the reactions were analyzed by elemental analysis (**Table 4**) and IR measurements (**Figure 6**). The amount of deposited carbon was in the following order: SMA-3 < ZSM-5 < N631-L < USY. Hydrogen was also detected, whereas trace amounts of nitrogen and sulfur were observed. The molar ratio of hydrogen to carbon (H/C) on USY was <1, indicating that the adsorbed hydrocarbons were polyaromatics (PAHs). H/C on SMA-3 and N631-L was close to 2, and therefore alkanes or long-chain alkylaromatics were presumed to be formed. ZSM-5 showed higher H/C than the other catalysts. IR spectra of the catalysts after the reaction indicated the existence of aromatics and alkanes. An absorption band at 1600 cm^{-1} was assigned to C=C stretching vibration in aromatics, and the absorbance was in the following order: USY > ZSM-5 > N631-L > SMA-3. A pair of absorption bands at 2850 and 2900 cm^{-1} was assigned to C-H stretching vibration in alkanes and/or alkyl groups (in alkylaromatics) and observed in all the spectra. The deposited substances on USY are thus revealed to have been predominantly PAHs, while the substances on N631-L and SMA-3 were alkanes and small amounts of alkylaromatics. The adsorbed substances on ZSM-5 were mostly alkyl aromatics; too high a H/C ratio suggests the presence of water condensed in the micropores.

3.3. Influence of textural property of SMA on activity and selectivity in the dealkylation

As stated in the last section, SMA efficiently catalyzed the dealkylation of APAHs into PAHs and long-chain alkanes. As previously reported, the activity of SMA for the dealkylation of a model substance was created by the deposition of silica monolayer with Brønsted acidity, and the activity showed the maximum on the catalyst where the coverage by the monolayer was the maximum, presumably due to high density of Brønsted acid

sites⁶. Therefore, the importance of Brønsted acidity is undoubtable for the activity of SMA in the dealkylation of APAHs. However, the low selectivity of amorphous silica-alumina (mesoporous) and zeolites (microporous) as shown in the last section suggests the influence of the porous nature on this reaction. It is presumed that the textural properties of the catalyst affected the activity for the dealkylation of APAHs in the practical VGO, which contained bulk hydrocarbon molecules, and their diffusion was prevented to some extent. Accordingly, the pore size of SMA was varied, and its influence was investigated. SMA-1 to -4 were prepared by the deposition of silica monolayer on γ -alumina samples with different pore sizes from 6 to 33 nm; the resultant pore sizes of SMA were similar to the pore sizes of the support alumina samples (**Table 1** and **Table S1**). The number of Brønsted acid sites normalized by catalyst weight or surface area was not largely different (within 0.06-0.11 mol kg⁻¹ or 0.25-0.36 nm⁻²), as well, Brønsted acid strength (ΔH) was similar as shown in **Table 3**. The similar acidic properties suggest a principally same chemical nature of SMA surface due to equivalent microstructure. It is concluded that the SMA-1 to -4 had similar microstructures and Brønsted acidic properties, but the porous nature at 1-10 nm dimensions was different.

The activities of SMA in the dealkylation are shown in **Figures S8-S11**. The composition of components in the reactions over all the catalysts displayed analogous changes over the time on stream, and was steady during 5-8 h. **Figure 7** shows the average composition of components during 5-8 h in the dealkylation over SMAs. Both the APAHs and PAHs were retrieved in the same amount over all the SMAs. This tells us that the dealkylation activities of all the SMA catalysts were comparable. The amount of alkylbenzenes after the reaction was almost the same as the original amount in VGO. Long-chain alkanes (>C₂₀) relatively decreased over SMA-1 and -2, compared with SMA-3 and -4, while the composition of light hydrocarbons was in the following order: SMA-2 > -1 > -3 > -4. There were no differences in yield of C₁₀₋₂₀ and C₅₋₉ alkanes among all the catalysts. A part of long-chain alkanes was thus observed to be cracked into C₅₋₉ alkanes, but deep cracking into C₁₋₆ alkanes proceeded only on the SMA with relatively small mesopore size.

4. Discussion

The assumed novel upgrading process consists of the dealkylation of APAHs in the feed mixture and the separation of aromatics (polar) and alkanes (non-polar) based on the large difference in polarity. The alkyl aromatic

molecules possessing long alkyl chains with high compatibility should hinder the polar separation. Therefore, they need to be completely dealkylated. Alkanes are usually contained in the feed oil and produced by the dealkylation. Among the alkanes, the C5-10, C10-20, and larger alkanes are utilized as gasoline, diesel fuel, and lubricating oil, respectively, while the short chain (<C4) alkanes, i.e., off-gas, are useless. The long-chain alkanes can be converted into alkanes suitable for gasoline and diesel fuel, and monocyclic aromatics by the conventional FCC if necessary, while the off-gas components are difficult to convert into valued compounds. Therefore, in the dealkylation step, the chain length of alkanes and alkyl groups in the alkyl aromatics should be kept; therefore, cracking of alkanes, a side reaction, needs to be restricted, and high yield of long-chain alkanes is desirable. For the above reactions, this research target is to find the catalyst which shows high conversion of APAHs and selectivity of long-chain alkanes in the dealkylation. High HDN conversion and decrease of recovered APAHs show high catalytic activity for the desired reaction (dealkylation of APAH), while production of large amounts of recovered long-chain alkanes (C10-20 for diesel fuel and >C20 for lubricating oil) and small amounts of recovered C5-9 alkanes and light hydrocarbons shows the high selectivity for the desired reaction.

HDN conversion was in the order ZSM-5 < USY < SMA-3 < N631-L, while amounts of recovered APAHs were SMA-3 < N631-L \approx USY < ZSM-5. HDN conversion on SMAs gradually decreased in **Figures 1** and **S8**. The catalysts were deactivated by the adsorption of long-chain alkanes, but the deactivated catalysts can be regenerated by calcination at 773 K in oxygen flow ⁷. No difference among the SMAs was found in HDN conversion and amounts of recovered APAHs. In addition, the order of amounts of recovered alkylbenzenes was SMA-3 < N631-L < USY \ll ZSM-5; the amount of alkylbenzenes increased from the original VGO on catalysts other than SMAs, indicating the formation of alkylbenzenes. Amount of total recovered long-chain alkanes (C10-20 and >C20) was in the following order: ZSM-5 < USY < N631-L < SMA-3. In light alkanes, C5-9 alkanes were produced in the order ZSM-5 < SMA-3 \approx USY < N631-L, while yield of light hydrocarbons was SMA-3 < N631-L < USY < ZSM-5. Total images of the reactions on the catalysts are shown in **Figure S12**. The bracketed values were calculated on the basis of **Tables S2-5** and averaged over 5-8 h in the reactions. The width of the arrows in the images indicates the amount of changes of hydrocarbons. SMA-3 reduced more APAHs and HDN (a total of 7.6 wt% from 30.6 c-mol%) and showed more yield of >C20 alkanes (45.7 c-mol%), indicating that SMA-3

exhibited high dealkylation activity and high selectivity of long-chain alkanes. N631-L and USY showed higher yield of short-chain alkanes (C5-9 alkanes and light hydrocarbons) than SMA-3, due to the cracking of alkanes. ZSM-5 showed higher yield of APAHs and HDN, but less yield of >C20 and C10-20 alkanes (a total of 16.8 c-mol%) than the other catalysts. In comparison by SMA, >C20 alkanes were less over SMA-1 and -2 than SMA-3 and -4, while yield of light hydrocarbons was in the following order: SMA-4 < -3 < -1 < -2. However, there were no differences in yield of C10-20 and C5-9 alkanes among the SMAs.

The pore size was found to be ZSM-5 < USY < N631-L < SMAs, while the Brønsted acid strength was SMAs < N631-L < USY < ZSM-5. Among SMAs, mode value of pore size was in the order SMA-1 < -2 < -3 < -4, whereas all the catalysts possessed a similar amount and strength of Brønsted acid sites.

The previous studies revealed high activity of SMAs in the dealkylation of model APAH reactant^{6,7}. This study confirms the higher conversion of APAHs in the practical oil and selectivity of long-chain alkanes on SMAs than amorphous silica-alumina and zeolites. The high conversion on SMAs is related to the large pore size. It is supposed that the bulky reactant molecules can penetrate into the large pore of SMAs and then be dealkylated into alkanes and PAHs. On the other hand, the cracking of alkane is more difficult, from the viewpoint of acid-catalysis chemistry, than dealkylation of alkyl aromatics, because it needs a strong Brønsted acid site as follows. The dealkylation of APAHs proceeds through attack of H⁺ on the aromatic ring and then formation of the carbenium ion (arenium ion) for relatively stable intermediates of σ -complex, and finally produces PAHs and alkenes (subsequently hydrogenated into alkanes). The aromatic rings are subject to nucleophilic attack, and therefore the dealkylation proceeds on even weak Brønsted acid sites. On the other hand, cracking of alkane proceeds through formation of an alkanium ion by attack of H⁺ and then the protolytic cracking into a carbenium ion and an alkane (or a dihydrogen). Alkanium ion is an unstable intermediate, and therefore the cracking proceeds on only strong Brønsted acid sites. Weak Brønsted acid sites on SMAs cannot catalyze the cracking of both alkanes and alkyl groups in APAHs. According to these explanations, the high selectivity (low activity for alkane cracking) of SMA is considered to be due to the moderate Brønsted acid strength, and alkyl groups in the reactants and the produced alkanes were difficult to crack into lighter alkanes. Thus, the large pore size and moderate Brønsted acid strength are concluded to generate the high activity and selectivity of SMA for the dealkylation of APAHs.

A difference between APAHs and alkylbenzenes was observed in the reaction over SMAs; the SMA was inactive for the dealkylation of alkyl monocyclic aromatics but active for the dealkylation of APAHs. The arenium ion formed from APAHs holds a higher variety of resonance structures than that formed from alkylbenzenes. Due to the higher stability of the intermediate, the APAHs should be more reactive than the alkylbenzenes. As a result, the SMA catalyzed the conversion of APAHs but kept the alkylbenzene, which is directly useful for chemical resources, adding an advantage of the presently proposed process using SMA.

A part of APAHs remained on even SMAs, but most of them consisted of short (C1-4) alkyl groups. Binding energy between alkyl groups and aromatic rings is in the following order: propyl < ethyl << methyl³⁴. In addition, the carbenium ion formed by the dealkylation is stable in the following order: tertiary carbon > secondary carbon > primary carbon > methylium. From the above principles, the removal of methyl and ethyl groups from the aromatic ring is estimated to be difficult compared to the >C3 alkyl groups. It is therefore reasonable to conclude that methyl and ethyl groups, in some cases multiple ones in a molecule, were unreacted on SMA and detected as the APAHs with C1-4 alkyl groups. The purpose of dealkylation is to separate the aromatic rings from alkanes which are useful as fuel and/or the feeds of further treatment. The long-chain alkanes are useful as fuels and/or feeds, but C1-4 alkanes are not, and therefore the observed inactivity of C1-4 alkyl groups does not reduce the advantages of SMA for the dealkylation of APAHs.

N631-L and USY formed more APAHs in the initial period than during 6-8 h. The dealkylation of APAHs and the cracking of alkanes probably proceeded, and then polymerization to APAHs deactivated a part of the acid sites such as strong Brønsted acid sites. However, only the dealkylation proceeded with time. On the other hand, ZSM-5 substantially catalyzed cracking of long-chain alkanes and produced lighter alkanes along with formation of alkylbenzenes by swift cyclization of alkenes. N631-L exhibited higher activity in the dealkylation than SMAs (**Figures 1 and 2**) but formed APAHs by the cracking and polymerization of alkanes in the initial period (**Figure 2**). Therefore, the order of conversion in **Figure 1** was different from the order of composition of APAHs in **Figure 2**. However, carbon deposition on ZSM-5 also deactivated the acid sites, and the reaction rate in the dealkylation of APAHs decreased with the time on stream. From the above results, APAHs on N631-L, USY, and ZSM-5 were recovered more than SMAs, and the cracking of long-chain alkanes proceeded.

SMA-1 and SMA-2 exhibited the same dealkylation activity, but a difference of alkane selectivity was observed. The selectivity of long-chain alkanes (>C₂₀) on SMA-1 and -2 was less than that on SMA-3 and -4, while the composition of light hydrocarbons was in the following order: SMA-2 > -1 > -3 > -4. It was speculated that long-chain alkanes were prone to contact with acid sites due to high surface area on SMA-1 and -2, otherwise due to capillary condensation in the smaller mesopores in SMA-1 and -2 than that in SMA-3 and -4. Therefore, SMA-3 and -4, which had weak Brønsted acid sites and large pores, exhibited higher dealkylation activity and selectivity of long-chain alkanes than the other solid acids including SMA-1 and -2. However, the pore size did not determinately influence the dealkylation activity. Therefore, production of SMA catalysts for dealkylation should be commercially practicable.

5. Conclusions

A silica-monolayer loaded on alumina (SMA) with weak Brønsted acid sites and large pore size catalyzed dealkylation of APAHs in a practical heavy oil such as VGO, and exhibited higher activity and selectivity of long-chain alkanes than amorphous silica-alumina (N631-L) and the zeolites (USY and ZSM-5). High activity on SMAs was proposed to be due to larger pore size in which APAHs could sufficiently diffuse. Some APAHs were retrieved, but combined with multiple methyl or ethyl groups. The residual should not affect separation of alkanes and PAHs by solvent extraction. On the other hand, the produced alkanes and alkyl groups in the reactants were not cracked on weak Brønsted acid sites in SMAs. The retrieved >C₂₀ and C₁₀₋₂₀ alkanes can be utilized as lubricating oil and light oil or kerosene, respectively. On the hand, C₅₋₉ alkanes and light hydrocarbons were hardly formed. Analyses of SMA after the reaction found adsorbed alkanes, which did not lead to drastic deactivation. Additionally, pore size of SMA increased with limiting cracking of long-chain alkanes, and the catalysts with larger pores exhibited higher selectivity of long-chain alkanes. The dealkylation produced long-chain alkanes and PAHs, which can be converted to benzene derivatives through further treatment. Catalytic reforming of long-chain alkanes may form benzene, toluene, and xylenes, whereas PAHs are converted into tetralin derivatives through partial hydrogenation, and further ring-opening of the naphthene in tetralin derivatives produces benzene and its derivatives. These processes for production of the aromatics will be studied as future work.

Conflicts of interest

There are no conflicts to declare.

Acknowledgements

A part of this work was carried out as a part of projects for technological development entrusted by Ministry of Economy, Trade and Industry, Japan to Japan Petroleum Energy Center. The other part was supported by JSPS KAKENHI Grant Number 16H04568, and JST CREST Grant Number JPMJCR17P1, Japan.

References

-
- ¹ J. Chang, N. Tsubaki and K. Fujimoto, *Fuel*, 2001, **80**, 1639–1643.
 - ² R. Yoshida, M. Miyazawa, H. Ishiguro, S. Itoh, K. Haraguchi, H. Nagaishi, H. Narita, T. Yoshida, Y. Maekawa and Y. Mitarai, *Fuel Process. Technol.*, 1997, **51**, 195–203.
 - ³ R. Yoshida, M. Miyazawa, T. Yoshida, H. Narita and Y. Maekawa, *Fuel*, 1996, **75**, 99–102.
 - ⁴ R. Yoshida, T. Yoshida, H. Narita and Y. Maekawa, *Fuel*, 1986, **65**, 425–428.
 - ⁵ Organization of the Petroleum Exporting Countries, World Oil Outlook 2019.
 - ⁶ N. Katada, Y. Kawaguchi, K. Takeda, T. Matsuoka, N. Uozumi, K. Kanai, S. Fujiwara, K. Kinugasa, K. Nakamura, S. Suganuma and M. Nanjo, *Appl. Catal. A Gen.*, 2017, **530**, 93–101.
 - ⁷ K. Kinugasa, F. Nakano, S. Nagano, S. Suganuma, E. Tsuji and N. Katada, *J. Japan Pet. Inst.*, 2018, **61**, 294–301.
 - ⁸ S. Suganuma, K. Arita, F. Nakano, E. Tsuji and N. Katada, *Fuel*, 2020, **266**, 117055.
 - ⁹ K. Nakajima, S. Suganuma, E. Tsuji and N. Katada, *React. Chem. Eng.*, **5**, 1272–1280.
 - ¹⁰ S. Suganuma and N. Katada, *Fuel Process. Technol.*, 2020, **208**, 106518.
 - ¹¹ S. W. Ferris, E. R. Birkhimer and L. M. Henderson, *Ind. Eng. Chem.*, 1931, **23**, 753–761.
 - ¹² A. De Lucas, L. Rodriguez, P. Sanchez and A. Carnicer, *Sep. Sci. Technol.*, 1993, **28**, 2465–2477.
 - ¹³ B. Coto, R. van Grieken, J. L. Peña and J. J. Espada, *Chem. Eng. Sci.*, 2006, **61**, 8028–8039.
 - ¹⁴ B. W. Wojciechowski, *Catal. Rev.*, 1982, **24**, 1–65.
 - ¹⁵ A. M. Youssef, A. I. Ahmed and S. E. Samra, *Mater. Lett.*, 1990, **10**, 175–180.
 - ¹⁶ M. Du, Z. Qin, H. Ge, X. Li, Z. Lü and J. Wang, *Fuel Process. Technol.*, 2010, **91**, 1655–1661.
 - ¹⁷ A. Stanislaus and H. C. Barry, *Catal. Rev.*, 1994, **36**, 75–123.
 - ¹⁸ Y. Choi, J. Lee, J. Shin, S. Lee, D. Kim and J. K. Lee, *Appl. Catal. A Gen.*, 2015, **492**, 140–150.
 - ¹⁹ A. Corma, V. González-Alfaro and A. V. Orchillés, *J. Catal.*, 2001, **200**, 34–44.
 - ²⁰ M. Santikunaporn, J. E. Herrera, S. Jongpatiwut, D. E. Resasco, W. E. Alvarez and E. L. Sughrue, *J. Catal.*,

2004, **228**, 100–113.

- ²¹ J. Shin, Y. Oh, Y. Choi, J. Lee and J. K. Lee, *Appl. Catal. A Gen.*, 2017, **547**, 12–21.
- ²² Y. Oh, J. Shin, H. Noh, C. Kim, Y. S. Kim, Y. K. Lee and J. K. Lee, *Appl. Catal. A Gen.*, 2019, **577**, 86–98.
- ²³ Y. Oh, H. Noh, H. Park, H. Han, T. B. Nguyen and J. K. Lee, *Catal. Today*, 2020, **352**, 329–336.
- ²⁴ M. Niwa, T. Hibino, H. Murata, N. Katada and Y. Murakami, *J. Chem. Soc. Chem. Commun.*, 1989, 289–290.
- ²⁵ M. Niwa, N. Katada and Y. Murakami, *J. Phys. Chem.*, 1990, **94**, 6441–6445.
- ²⁶ S. Brunauer, P. H. Emmett and E. Teller, *J. Am. Chem. Soc.*, 1938, **60**, 309–319.
- ²⁷ E. P. Barrett, L. G. Joyner and P. P. Halenda, *J. Am. Chem. Soc.*, 1951, **73**, 373–380.
- ²⁸ M. Niwa, S. Inagaki and Y. Murakami, *J. Phys. Chem.*, 1985, **89**, 3869–3872.
- ²⁹ M. Niwa, K. Suzuki, N. Katada, T. Kanougi and T. Atoguchi, *J. Phys. Chem. B*, 2005, **109**, 18749–18757.
- ³⁰ S. Suganuma, Y. Murakami, J. Ohyama, T. Torikai, K. Okumura and N. Katada, *Catal. Letters*, 2015, **145**, 1904–1912.
- ³¹ N. Katada, T. Tsubaki and M. Niwa, *Appl. Catal. A Gen.*, 2008, **340**, 76–86.
- ³² N. Katada, T. Fujii, K. Iwata, Y. Hibino and M. Niwa, *J. Catal.*, 1999, **186**, 478–480.
- ³³ M. Niwa and N. Katada, *Chem. Rec.*, 2013, **13**, 432–455.
- ³⁴ M. Szwarc, *Chem. Rev.*, 1950, **47**, 75–173.

Table 1 Physical properties of the silica-monolayer deposited on alumina

Catalyst	Al ₂ O ₃	Amount of SiO ₂ ^{*1} / wt%	Deposited Si atoms / nm ⁻²	Coverage / %	Surface area ^{*2} / m ² g ⁻¹	Pore size ^{*3} / nm	Mesopore volume ^{*4} / cm ³ g ⁻¹
SMA-1	Purchased	14.1	8.5	86	184 ^{*6}	6.2	0.36 ^{*6}
	sample ^{*5}				(214 ^{*7})		(0.42 ^{*7})
SMA-2	ALO-9	14.2	8.1	90	182 ^{*6} (212 ^{*7})	9.2	0.58 ^{*6} (0.68 ^{*7})
SMA-3	ALO-6	13.3	7.9	91	169 ^{*6} (195 ^{*7})	24	0.83 ^{*6} (0.96 ^{*7})
SMA-4	ALO-7	13.1	8.7	95	147 ^{*6} (169 ^{*7})	33	0.95 ^{*6} (1.09 ^{*7})

^{*1} Normalization by catalyst weight, ^{*2} calculated by BET equation, ^{*3} mode value of pore size calculated by BJH method, ^{*4} calculated by BJH method, ^{*5} sample purchased from FUJIFILM Wako Pure Chemical Corp., ^{*6} normalized by catalyst weight, ^{*7} divided by the weight of alumina as a support.

Table 2 Physical properties of amorphous silica-alumina and zeolites

Catalyst	Surface area ^{*1} / m ² g ⁻¹	Pore size / nm	Micropore volume ^{*2} / cm ³ g ⁻¹	Mesopore volume ^{*3} / cm ³ g ⁻¹
N631-L	483	3.7 ^{*4}	<0.01	0.51
USY	756	0.74 × 0.74 ^{*5}	0.30	0.24
ZSM-5	308	0.53 × 0.56, 0.55 × 0.51 ^{*5}	0.13	0.12

^{*1} Calculated by BET equation, ^{*2} calculated using *t*-plot method, ^{*3} calculated by BJH method, ^{*4} mode value of pore size calculated by BJH method, ^{*5} estimated by crystal structures of zeolite.

Table 3 Acidic properties of solid acids

Catalyst	Brønsted acid amount	ΔH ^{*2}
	/ mol kg ⁻¹ (site nm ⁻²) ^{*1}	/ kJ mol ⁻¹
SMA-1	0.11 (0.36)	116
SMA-2	0.08 (0.26)	116
SMA-3	0.10 (0.36)	116
SMA-4	0.06 (0.25)	116
N631-L	0.17 (0.21)	122
USY	0.34 (0.27)	136
ZSM-5	1.14 (2.23)	148

^{*1} Number of Brønsted acid sites normalized by BET surface area, ^{*2} mode value in enthalpy of ammonia desorption from Brønsted acid sites.

Table 4 Elemental analysis of adsorbed substances on the catalysts after the dealkylation of APAHs in fed VGO after 8 h time-on-stream at 723 K.

	wt%				Molar ratio
	C	H	N	S	H/C
SMA-3	5.43	0.80	Trace	Trace	1.77
N631-L	13.85	5.10	Trace	Trace	1.82
USY	22.09	1.56	Trace	Trace	0.85
ZSM-5	6.84	1.54	Trace	Trace	2.70

Figure Captions

- Figure 1 Time courses of HDN (hexadecylnaphthalene) conversion on SMA-3 (●), N631-L (■), USY (◇), and ZSM-5 (Δ) in the dealkylation of APAHs in fed VGO at 723 K and $LHSV = 5.7 \text{ g}_{VGO} \text{ g}_{cat}^{-1} \text{ h}^{-1}$.
- Figure 2 Time courses of composition of APAHs in products on SMA-3 (●), N631-L (■), USY (◇), and ZSM-5 (Δ) in the dealkylation of APAHs in fed VGO at 723 K and $LHSV = 5.7 \text{ g}_{VGO} \text{ g}_{cat}^{-1} \text{ h}^{-1}$. Double circle means the amount of APAHs in the original (fed) VGO.
- Figure 3 Time courses of composition of alkylbenzenes in products on SMA-3 (●), N631-L (■), USY (◇), and ZSM-5 (Δ) in the dealkylation of APAHs in fed VGO at 723 K and $LHSV = 5.7 \text{ g}_{VGO} \text{ g}_{cat}^{-1} \text{ h}^{-1}$. Double circle means the amount of alkylbenzenes in the original (fed) VGO.
- Figure 4 Time courses of composition of alkanes ((A): >C20, (B): C10-20, and (C): C5-9) in products on SMA-3 (●), N631-L (■), USY (◇), and ZSM-5 (Δ) in the dealkylation of APAHs in fed VGO at 723 K and $LHSV = 5.7 \text{ g}_{VGO} \text{ g}_{cat}^{-1} \text{ h}^{-1}$. Double circle means the amounts of alkanes in the original (fed) VGO.
- Figure 5 Composition of light hydrocarbons averaged during 2-8 h in the dealkylation of APAHs in fed VGO at 723 K and $LHSV = 5.7 \text{ g}_{VGO} \text{ g}_{cat}^{-1} \text{ h}^{-1}$.
- Figure 6 IR spectra of various solid acids after the dealkylation of APAHs in fed VGO after 8 h time on stream at 723 K. Red line: SMA-3, blue line: N631-L, green line: USY, and purple line: ZSM-5.
- Figure 7 Compositions of outlet compounds averaged during 5-8 h on SMAs in the dealkylation of APAHs in fed VGO at 723 K and $LHSV = 5.7 \text{ g}_{VGO} \text{ g}_{cat}^{-1} \text{ h}^{-1}$. The compositions in the original (fed) VGO are shown in a leftmost bar.

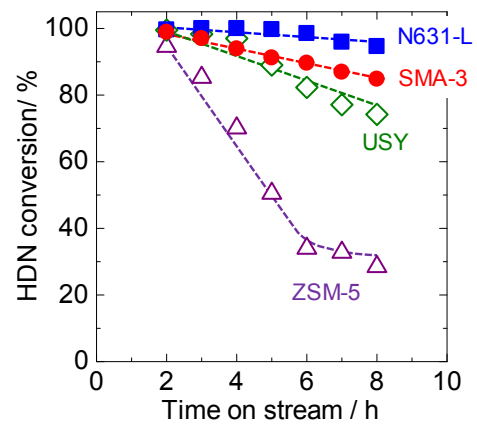


Figure 1

Alkyl polyaromatic hydrocarbons

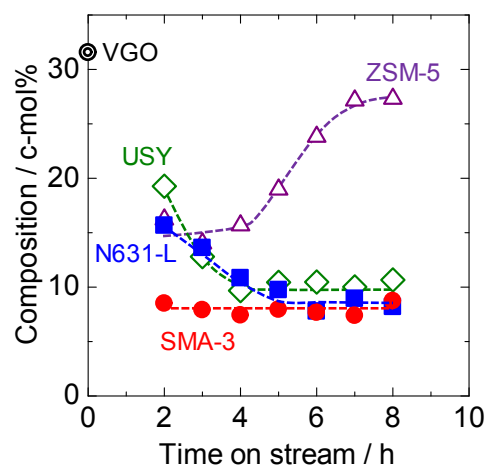


Figure 2

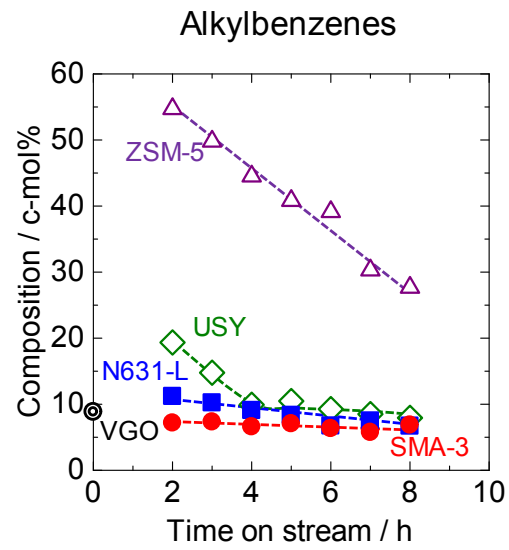


Figure 3

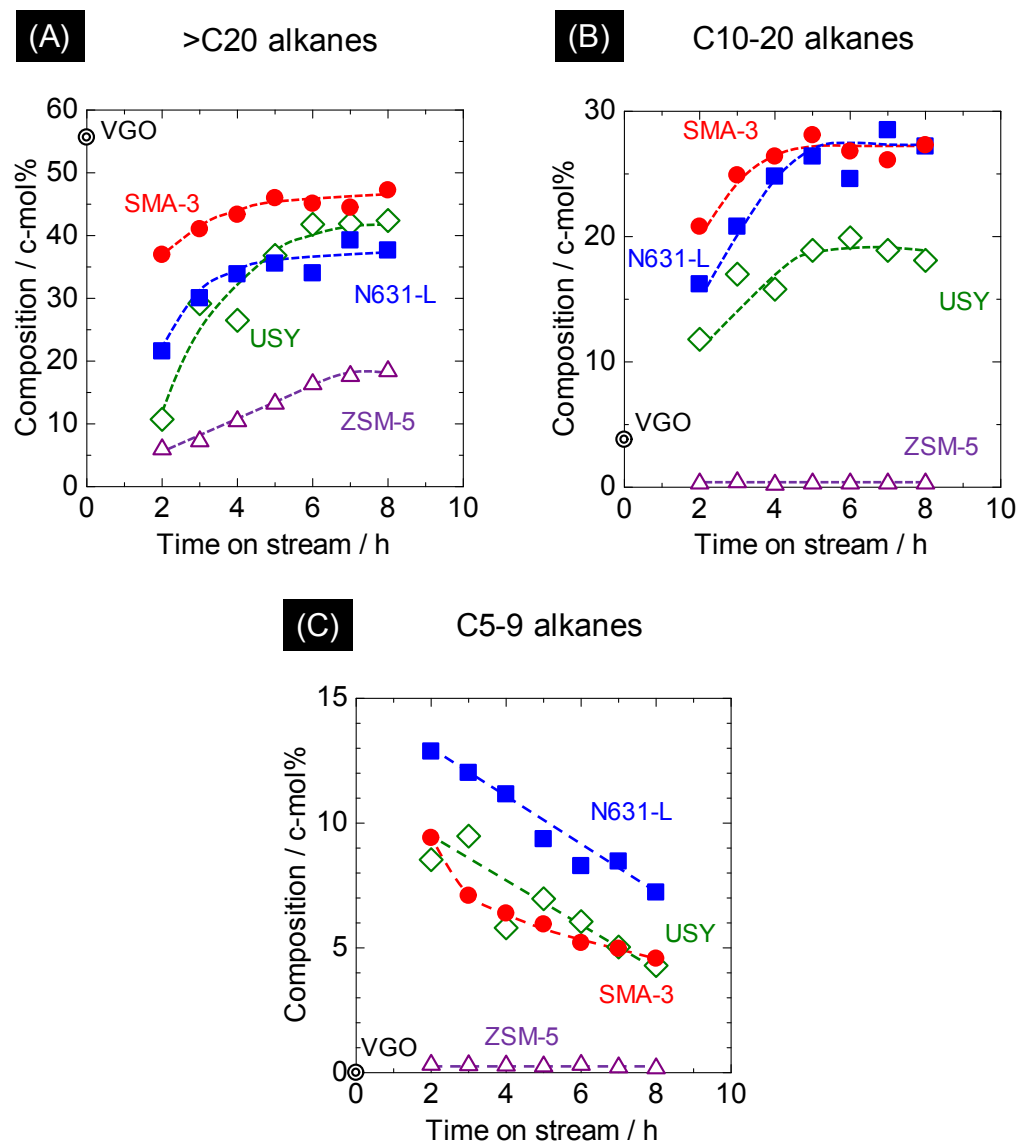


Figure 4

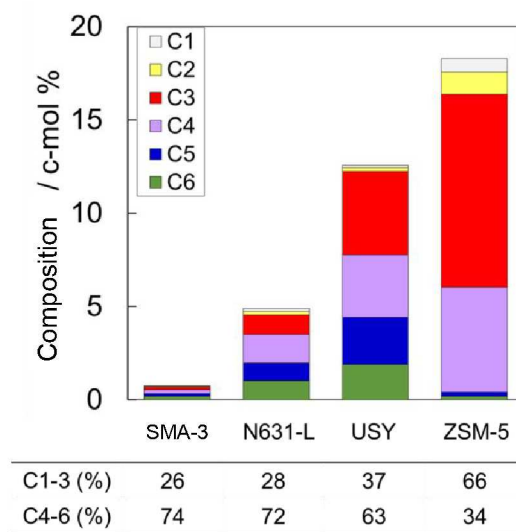


Figure 5

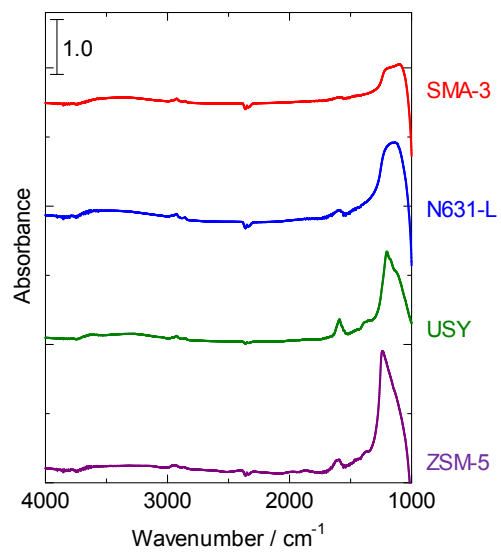


Figure 6

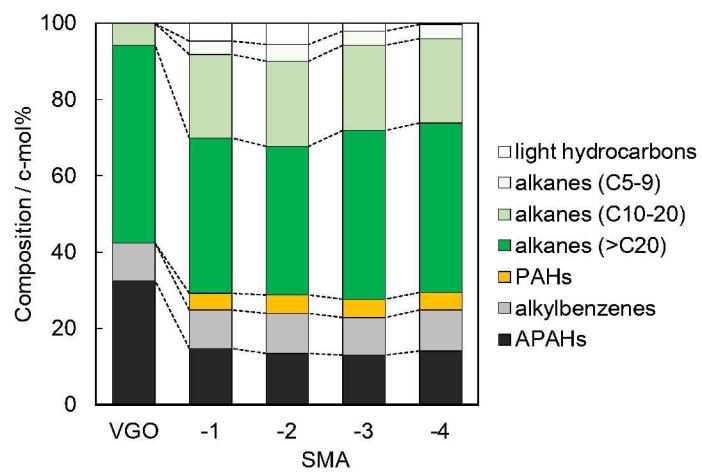
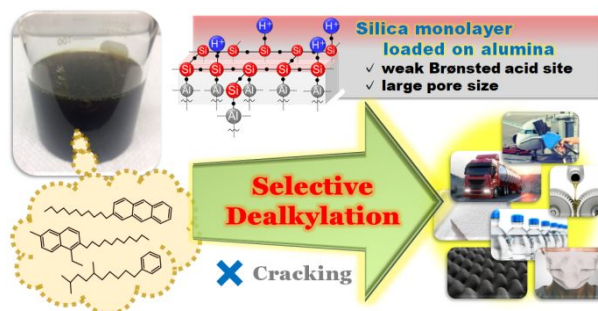


Figure 7



Silica-monolayer loaded on alumina with weak Brønsted acid sites and large pore size can selectively dealkylate alkyl polycyclic aromatics to long-chain alkanes and polycyclic aromatics for chemicals and fuel.